

Indication of nearby source signatures of cosmic rays from energy spectra and anisotropies

Wei Liu^a, Yi-Qing Guo^{*a} and Qiang Yuan^{†b,c,d}

^a*Key Laboratory of Particle Astrophysics, Institute of High Energy Physics, Chinese Academy of Sciences, Beijing 100049, China*

^b*Key Laboratory of Dark Matter and Space Astronomy, Purple Mountain Observatory, Chinese Academy of Sciences, Nanjing 210008, China*

^c*School of Astronomy and Space Science, University of Science and Technology of China, Hefei 230026, China*

^d*Center for High Energy Physics, Peking University, Beijing 100871, China*

October 22, 2019

Abstract

The origin of Galactic cosmic rays (GCRs) remains a mystery after more than one century of their discovery. The diffusive propagation of charged particles in the turbulent Galactic magnetic field makes us unable to trace back to their acceleration sites. Nevertheless, nearby GCR source(s) may leave imprints on the locally measured energy spectra and the anisotropies of the arrival direction. In this work we propose a simple but natural description of the GCR production and propagation, within a two-zone disk-halo diffusion scenario together with a nearby source, to understand the up-to-date precise measurements of the energy spectra and anisotropies of GCRs. We find that a common energy scale of ~ 100 TeV appears in both energy spectra of protons and helium nuclei measured recently by CREAM and large-scale anisotropies detected by various experiments. These results indicate that one or more local sources are very likely important

*Corresponding author: guoyq@ihep.ac.cn

†Corresponding author: yuanq@pmo.ac.cn

contributors to GCRs below 100 TeV. This study provides a probe to identify source(s) of GCRs by means of joint efforts of spectral and anisotropy measurements.

1 Introduction

It is widely postulated that GCRs below the so-called knee are mainly accelerated by supernova remnants (SNRs), through the well-known diffusive shock acceleration process [1, 2]. A power-law spectrum is expected to be produced at the acceleration source, i.e., $dN/d\mathcal{R} \propto \mathcal{R}^{-\nu}$, with \mathcal{R} being the rigidity of the particle. The diffusive transport of GCRs in the Milky Way further softens the spectrum by $\mathcal{R}^{-\delta}$ with $\delta \approx 0.3 \sim 0.5$, as suggested by the secondary-to-primary ratio of GCRs [3, 4]. This general picture successfully explains the basic observational properties of GCRs below \sim PeV, as well as diffuse γ -rays [5]. However, the GCR anisotropy [6, 7, 8, 9, 10] is for a long time an unresolved problem. The diffusion model predicts one order of magnitude higher of the anisotropies of the arrival directions of GCRs compared with the measurements [11]. Meanwhile the phase does not point to the Galactic center less than \sim 100 TeV as expected by the conventional diffusion model [10].

Recent precise measurements of the energy spectra of GCRs further challenge this simple picture, such as the spectral hardenings at $\mathcal{R} \sim 200$ GV [12, 13, 14, 15], and the spatial variations of the inferred energy spectra of GCRs in the Milky Way from Fermi-LAT diffuse γ -rays [16, 17]. These new results suggest in general a non-uniform diffusion scenario of GCRs in e.g., the disk and halo [18, 19]. This is quite natural that GCRs diffuse slower in the Galactic disk where the magnetic field is more turbulent than that in the halo. Importantly, it was shown that this two-zone disk-halo diffusion scenario can help reduce the predicted amplitude of the GCR anisotropies [19]. However, it is not a full solution of the anisotropy problem, since the phase is not satisfactorily reproduced.

Most recently the balloon-borne experiment CREAM reported new measurements of the GCR proton and helium spectra up to \sim 100 TeV, which revealed potential spectral softenings above \sim 20 TeV [20]. Evidence of similar features was also reported by the NUCLEON group [21]. It is interesting to note that the energy distribution of the anisotropy amplitude also becomes flat from \sim 10 TeV and then decreases to a minimum at \sim 100 TeV after that the anisotropy increases again [10]. The phase of the dipole component of the anisotropies changes from R.A. \sim 4 hrs around 100 GeV to about -6 hrs above 100 TeV. In particular, the phase changes suddenly at \sim 100 TeV,

which implies a paradigm shift at such an energy. The common features from 10 to 100 TeV of the GCR energy spectra and anisotropies suggest a common origin of them.

It has been proposed that the local magnetic field may regulate the anisotropies of GCRs due to the anisotropic diffusion, and may explain the large-scale anisotropy pattern [22, 23, 24, 25, 26]. To account for the energy dependence of the amplitude and phase of the dipole component of the large scale anisotropies, local source(s) may also be necessary [27, 28, 29, 30, 31, 32, 24, 25]. Some additional effects, such as the motion of the solar system with respect to the local interstellar medium and/or the possible limited reconstruction capabilities of ground-based experiments are employed to reproduce the observations [25].

In this work, we propose a simple picture, based on the spatially dependent propagation (SDP) scenario together with a local source, to account for the observational facts about the spectral features of GCRs and anisotropies. The SDP model is well-motivated by the latest observations on the γ -ray halos around pulsars by HAWC [33]. It has been shown that the SDP scenario can also suppress the dipole anisotropies of cosmic rays, and thus help reconcile the long-term discrepancy of the anisotropies between data and the canonical diffusion model [19]. We suggest that new observations of the spectral softenings of the GCR nuclei above 20 TeV provide additional support of this scenario.

2 Model

2.1 Spatially-dependent diffusion

The shape of the diffusive halo is usually approximated to be a cylinder. The radial boundary of this propagation halo is equivalent to the Galactic radius, i.e., $R = 20$ kpc, whereas its half thickness z_h is about a few kpc which needs to be determined by fitting the GCR data [4, 34]. Both GCR sources and the interstellar medium (ISM) chiefly spread within the Galactic disk, whose width z_s is set to be ~ 200 pc. Besides the diffusion effect, GCR particles may also go through convection, reacceleration, and fragmentation due to the collisions with the ISM. At low energies, GCR nuclei further lose their energies via the ionization and Coulomb scattering. The transport equation

is generally written as

$$\begin{aligned} \frac{\partial \psi}{\partial t} = & Q(\mathbf{r}, p) + \nabla \cdot (D_{xx} \nabla \psi - \mathbf{V}_c \psi) + \frac{\partial}{\partial p} \left[p^2 D_{pp} \frac{\partial \psi}{\partial p} \right] \\ & - \frac{\partial}{\partial p} \left[\dot{p} \psi - \frac{p}{3} (\nabla \cdot \mathbf{V}_c) \psi \right] - \frac{\psi}{\tau_f} - \frac{\psi}{\tau_r}, \end{aligned} \quad (1)$$

where $\psi = dn/dp$ is the CR density per particle momentum p at position \mathbf{r} , $Q(\mathbf{r}, p)$ is the source function, D_{xx} and D_{pp} are the diffusion coefficients in the space and momentum space (describing the reacceleration), \mathbf{V}_c is the convection velocity, \dot{p} is the energy loss rate, τ_f and τ_r are the fragmentation and radioactive decaying time scales. At the border of the halo, free escape of CRs is assumed, namely $\psi(R, z, p) = \psi(r, \pm z_h, p) = 0$. For a comprehensive introduction to the CR transport, one can refer to [5, 35].

Following [19], the diffusion coefficient is assumed to be different in the inner halo ($|z| < \xi z_h$) and outer halo ($z \geq \xi z_h$), where $\xi \approx 0.1$ characterizes the thickness of the disk. In the inner halo region, which is close to the Galactic disk, the level of turbulence is appreciably affected by the activities of supernova explosions and expected to be intense. Recent HAWC observations have shown that the diffusion coefficient of GCRs within tens of parsecs around the source is at least two orders of magnitude smaller than the conventional one [33]. Since the filling factor of such slow diffusion regions is unclear, here we adopt a diffusion coefficient in the inner halo in between the HAWC-deduced value and the conventional one to approximate an average effect. In the outer halo, the turbulence is believed to be CR-driven and less affected by the stellar activities. The diffusion coefficient thus reduced to the conventional values. The diffusion parameters in the inner and outer halo are connected smoothly [19]. The parameterized diffusion coefficient adopted in this work is [19, 36]

$$D_{xx}(r, z, \mathcal{R}) = D_0 F(r, z) \left(\frac{\mathcal{R}}{\mathcal{R}_0} \right)^{\delta_0 F(r, z)}. \quad (2)$$

$F(r, z)$ is parameterized as

$$F(r, z) = \begin{cases} g(r, z) + [1 - g(r, z)] \left(\frac{z}{\xi z_0} \right)^n, & |z| \leq \xi z_0, \\ 1, & |z| > \xi z_0 \end{cases}, \quad (3)$$

in which $g(r, z) = N_m/[1 + f(r, z)]$, and $f(r, z)$ is the source density distribution. The spatial distribution of sources takes the form of SNR distribution [37], $f(r, z) \propto (r/r_\odot)^{1.69} \exp[-3.33(r - r_\odot)/r_\odot] \exp(-|z|/z_s)$, where $r_\odot = 8.5$

kpc and $z_s = 0.2$ kpc. The propagation equation of GCRs is solved with the DRAGON code [38]. The corresponding transport parameters are given in Table 1. The GCR secondary-to-primary ratios can be reasonably reproduced with these parameters [36].

The injection spectrum of background sources is assumed to be an exponential cutoff power-law form of rigidity, $q(\mathcal{R}) \propto \mathcal{R}^{-\nu} \exp(-\mathcal{R}/\mathcal{R}'_c)$. The cutoff rigidity, $\mathcal{R}'_c = 6.5$ PV, is tuned to fit the proton and helium spectra observed by KASCADE [39]. The injection power indexes and normalization fluxes at $E_k = 100$ GeV/n of heavier nuclei refer to [40], which are given in Table 2.

2.2 Local source

The propagation of particles from the local source is calculated using the Green's function method, assuming a spherical geometry with infinite boundary conditions. The GCR density as a function of space, rigidity, and time is

$$\phi(r, \mathcal{R}, t) = \frac{q_{\text{inj}}(\mathcal{R})}{(\sqrt{2\pi}\sigma)^3} \exp\left(-\frac{r^2}{2\sigma^2}\right), \quad (4)$$

where $q_{\text{inj}}(\mathcal{R})\delta(t)\delta(\mathbf{r})$ is the instantaneous injection spectrum of a point source, $\sigma(\mathcal{R}, t) = \sqrt{2D(\mathcal{R})t}$ is the effective diffusion length within time t , $D(\mathcal{R})$ is the diffusion coefficient which was adopted as the disk value described above. The injection spectrum is again parameterized as a cutoff power-law form, with a power-law index of 2.20 (2.15) for protons (helium nuclei) and a cutoff rigidity of ~ 60 TV. Note that in this work the local source is assumed to contribute mainly the proton and helium components of GCRs. The extension of this work to heavier nuclei can be found in an accompany work [41]. The normalization is determined through fitting the GCR energy spectra, which results in a total energy of $\sim 2 \times 10^{50}$ erg for protons and $\sim 1 \times 10^{50}$ erg for helium, which is about 30% of the shock kinetic energy of a typical core-collapse supernova. The distance and age of the local source are set to be $d = 330$ pc and $\tau = 3.4 \times 10^5$ years, which are the same as that inferred from the observations of Geminga [42, 43, 44].

3 Results

Figure 1 shows the energy spectra of protons and helium from the model predictions compared with the measurements by AMS-02 [15, 45], CREAM-III [20], NUCLEON [46], KASCADE [47] and KASCADE-Grande [39]. The red, blue and black lines represent the contributions from the local source,

the background sources and the sum of them, respectively. Due to the large measurement errors, the value of the cut-off rigidity of the local source contribution, \mathcal{R}_c , has large uncertainties. Here we set \mathcal{R}_c to be 30, 60 and 100 TV, and find that all of them are consistent with the measurements. As we will see below, the anisotropy features are more sensitive to the value of \mathcal{R}_c . As show in the figure, the background spectrum gradually flattens. This is attributed to the SDP effect. The diffusion coefficient and its rigidity dependence are assumed to be different in the disk and halo regions in the SDP model. Particularly, the diffusion coefficient depends more weakly on rigidity in the disk than in the halo. Therefore after propagation, the spectrum shows a gradually broken power-law form. We find that the recent measurements of the bump-like features of the energy spectra of protons and helium by CREAM [20] and NUCLEON [21] can be well reproduced in our model. Both measurements suggest spectral softenings above tens of TeV, which can be a signature of the local source component.

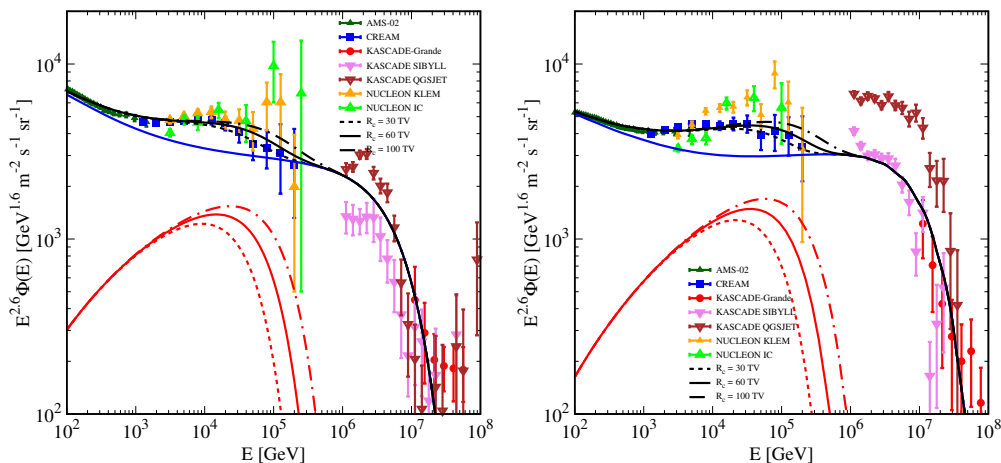


Figure 1: Energy spectra of protons (left) and helium nuclei (right). The data points are taken from AMS-02 [15, 45], CREAM-III [20], NUCLEON [46], KASCADE [47] and KASCADE-Grande [39] respectively. The blue lines are the background fluxes, the red lines are the fluxes from a nearby source located at (R.A. = $4^h 0^m$, $\delta = 24^\circ 30'$) with a distance of ~ 0.3 kpc, and the black lines are the sum of them. The dotted, solid, and dash-dotted lines are for three different cutoff rigidities, $\mathcal{R}_c = 30, 60,$ and 100 TV, respectively.

The amplitude and phase of the dipole anisotropy are shown in Figure 2. The anisotropy of GCRs depends on the sum of the GCR flows from the background (\mathbf{J}_{bkg}) and the local source ($\mathbf{J}_{\text{local}}$). \mathbf{J}_{bkg} points from the Galactic center to the anti-center, since GCR sources are more abundant

D_0	δ_0	N_m	ξ	n	v_A	z_h
$[\text{cm}^2 \cdot \text{s}^{-1}]$					$[\text{km} \cdot \text{s}^{-1}]$	$[\text{kpc}]$
4.46×10^{28}	0.62	0.4	0.1	4	6	5

Table 1: parameters of SDP model.

Element	Normalization [†]	ν	\mathcal{R}_c
	$[(\text{m}^2 \cdot \text{sr} \cdot \text{s} \cdot \text{GeV})^{-1}]$		$[\text{PV}]$
p	3.75×10^{-2}	2.40	6.5
He	2.4×10^{-3}	2.33	6.5
C	8×10^{-5}	2.35	6.5
O	9.8×10^{-5}	2.37	6.5
Mg	1.67×10^{-5}	2.33	6.5
Al	2.54×10^{-6}	2.35	6.5
Si	1.43×10^{-5}	2.44	6.5
Fe	1.37×10^{-5}	2.28	6.5

[†]The normalization is set at kinetic energy per nucleon $E_k = 100$ GeV/n.

Table 2: Injection parameters of the background sources.

in the inner Galaxy. The direction of the local source can be determined by the observational phase of the anisotropy, which suggests that the local source is located at the direction of the anti-Galactic center and is out of the Galactic disk. We find that a source located at (R.A. = $4^{\text{h}}0^{\text{m}}$, $\delta = 24^{\circ}30'$) gives very good fit to the measurements of both the amplitude and phase of the anisotropy. For $E < 100$ TeV, the local source contribution dominates the observed anisotropies, although its flux is sub-dominant. The phase thus keeps tracing the direction of the local source. Meanwhile since the energy spectra of $\mathbf{J}_{\text{local}}$ peak around 10 TeV, the amplitude of anisotropy also peak at such energies. For $E \gtrsim 100$ TeV, the contribution from the local source decreases significantly, and \mathbf{J}_{bkg} become dominant instead (see the red and blue lines in the bottom-left sub-panel of Figure 2 for $\mathbf{J}_{\text{local}}$ and \mathbf{J}_{bkg}). The phase of the dipole anisotropy turns to the direction of Galactic center. It is noteworthy that compared with the traditional diffusion model, the corresponding amplitude of CR anisotropy, which is dominated by the background \mathbf{J}_{bkg} , is naturally suppressed within a SDP model [19].

As a consistency check, we further calculate the all-particle spectra of GCRs, as shown in Figure 3. Here we do not consider nuclei heavier than helium for the local source. The model prediction is well consistent with the observational data [49].

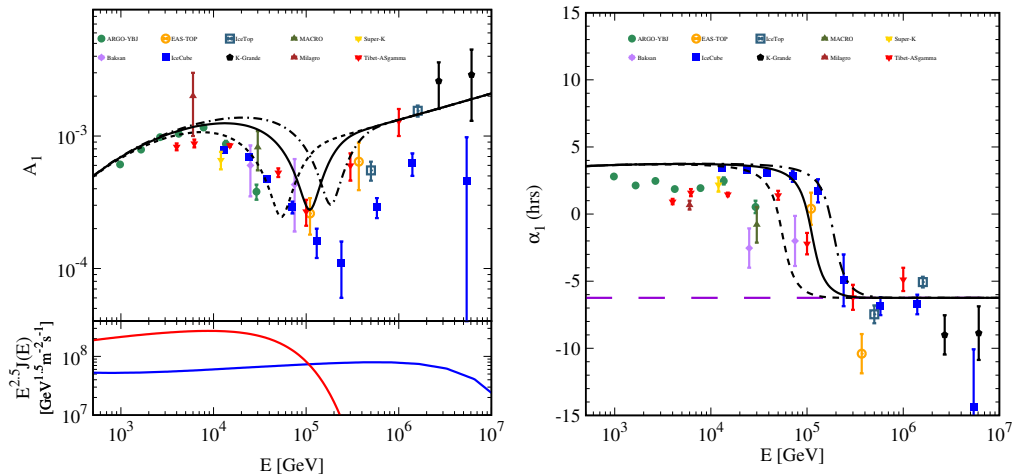


Figure 2: Energy dependences of the amplitude (left) and phase (right) of the dipole anisotropies. In the left panel, the three black lines correspond to the results for three different cutoff rigidities of the local source spectra (same as that in Figure 1). The blue and red lines in the lower sub-panel show the flows (defined as $J(E) = |D(E)\nabla\phi|$) of the background and local source (for the 60 TV cutoff case) components, respectively. In the right panel, the three black lines represent again the expected phase evolution for the three cutoff rigidities, and the purple long-dashed line shows the expectation of the background component, which points from the Galactic center to the anti-center. Observational data are taken from ref. [48] and references therein.

4 Discussion

After surveying the catalogues of local SNRs and pulsars, we find that the direction close to the Orion association (R.A. = 5^h30^m , $\delta = 10^\circ0'$), which is estimated to be the birthplace of the Geminga pulsar [42, 44], is close to the above required direction. Adopting the source location of the Orion association (about 330 pc [42, 44]), the amplitude and the phase of the anisotropy can be roughly reproduced, as shown in Figure 4. This result suggests that Geminga is probably the dominant source resulting in the spectral and anisotropy properties of GCRs from ~ 1 to 100 TeV.

Recent observations in the very-high-energy γ -ray band by the High Altitude Water Cherenkov (HAWC) observatory revealed extended emission around Geminga and another pulsar, which suggested a slow diffusion of GCR particles in a region of at least a few tens parsec around these pulsars [33]. Compared with the diffusion coefficient inferred from the secondary-to-primary ratio of GCRs [4], the HAWC observations suggest that the dif-

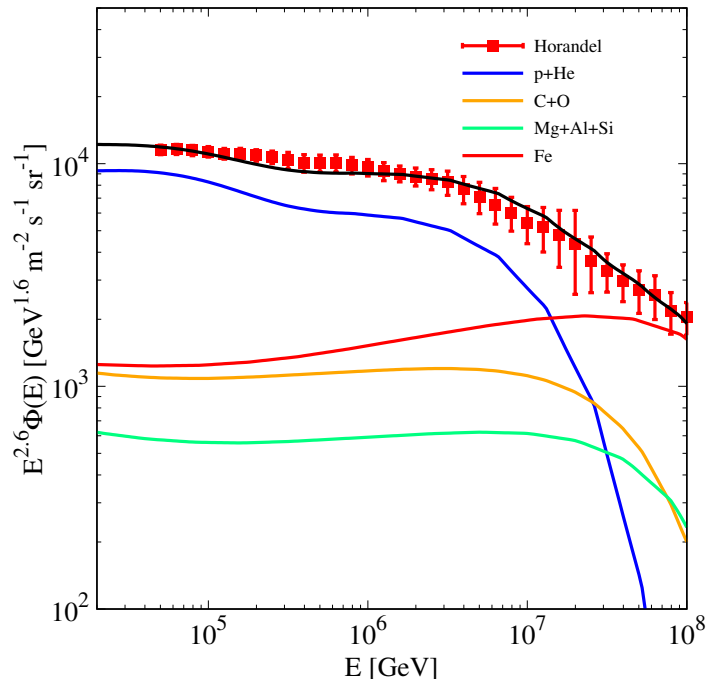


Figure 3: The all-particle spectra multiplied by $E^{2.6}$. The data points are taken from ref.[49]. The solid lines with different colors are the model predictions of different mass groups, and the black solid line is the total contribution.

fusion of particles in the Milky Way is non-uniform [50, 51]. Therefore the SDP scenario is supported by the HAWC data. Interestingly, the modeling of non-uniform diffusion of positrons in light of HAWC observations showed that Geminga can be a natural source of the positron anomaly [52, 53]. Our study further indicates that the SNR associated with Geminga could be the source of GCR nuclei, which gives rise to the spectral bumps around 10 TeV of the proton and helium spectra and the change of the anisotropy pattern around 100 TeV.

From Figure 4 we can see that the observational amplitude can be quite well reproduced, the phase at the low energy region (below 100 TeV) is not perfectly consistent with the data. It is possible that additional nearby sources other than Geminga also contribute to the anisotropies and/or spectra. This scenario should be natural. If SNRs are indeed the sources of GCRs, a simple estimate of SNRs in the local vicinity with proper distances and ages would lead to a number of a few, assuming a typical rate of Galactic supernovae [54]. We have added one additional source in the direction of

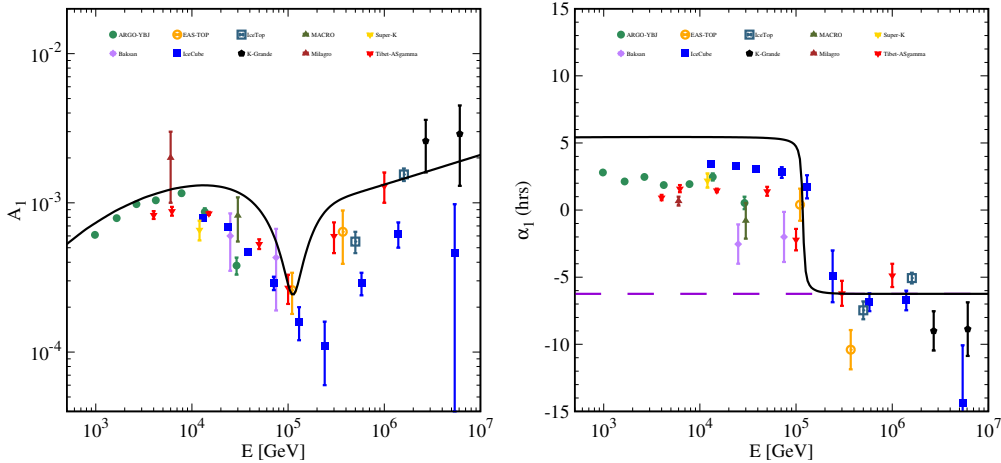


Figure 4: Amplitude (left) and phase (right) of the dipole anisotropies in the SDP scenario together with the contribution from Geminga (at its birth place).

(R.A. = 2^h31^m , $\delta = -8^\circ47'$), with a distance of 300 pc and an age of 3×10^5 years in the model. We find that the fit to the anisotropy phase can be improved with the anisotropy amplitude and GCR spectra almost unchanged. The results are shown in Figure 5.

It was proposed that the anisotropic diffusion due to the large-scale magnetic field might result in a projection of the GCR streaming along the direction of the magnetic field [22, 23, 24, 25, 26], which might account for the low energy ($\lesssim 100$ TeV) part of the anisotropies. Therefore, the possible projection effect of the anisotropies along the local magnetic field may improve the fit of the low energy anisotropy phase of the current model. Nevertheless, to what energies the projection effect gets to fail and the anisotropies start to reflect the source distribution may need further studies in order to properly reproduce the phase change around 100 TeV energies.

Finally, it is noteworthy that at $E \sim 100$ TeV, the variations of both the amplitude and phase of anisotropies are very sharp, which can be used as an energy calibration for ground-based experiments. Future experiments are expected to be able to measure the transition point around 100 TeV accurately.

5 Summary

In this work, we propose a two-zone diffusion scenario together with a nearby source to explain the energy spectra and anisotropies of GCRs. The spectral

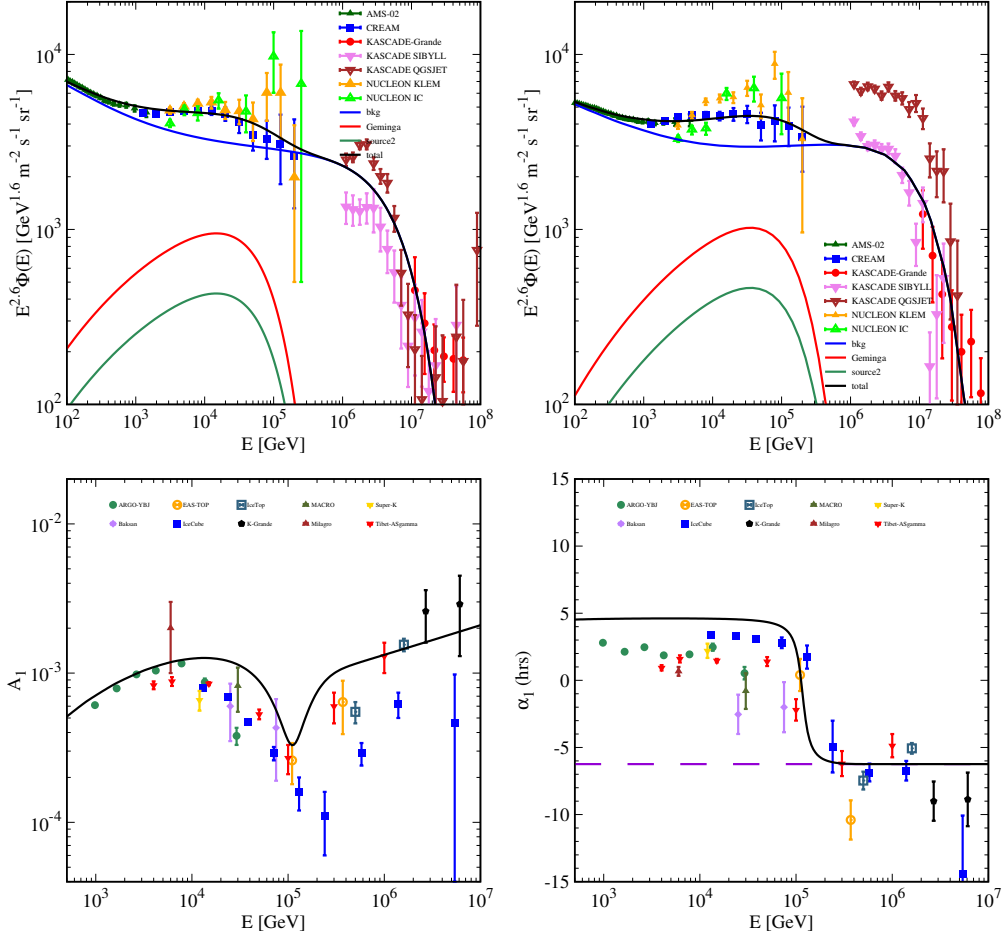


Figure 5: Energy spectra of protons (top left), helium nuclei (top right), and the amplitude (bottom left) and phase (bottom right) of the dipole anisotropies. The model consists of a background component and two local sources, Geminga (at its birth place) and a hypothetical source located at (R.A. = 2^h31^m , $\delta = -8^\circ47'$).

bumps of GCR protons and helium, reported recently by CREAM and NUCLEON, can be well fitted by a background component and a local source component of GCRs. The sum of the streamings of the background and local source components, can naturally explain the spectral evolutions of both the amplitude and phase of the dipole anisotropies. At low energies ($\lesssim 100$ TeV), the local source term dominates the GCR streaming and determines the low energy anisotropy pattern. From the phase of the dipole anisotropy, we propose that the SNR associated with Geminga may be an important candidate source forming the spectral features of GCR spectra

and anisotropies. For $E \gtrsim 100$ TeV, the background component dominates instead, and the anisotropy phase points from the Galactic center to the anti-center, and the amplitude increases with energies again following the diffusion law. The SDP scenario, as motivated by the HAWC observations of diffuse γ -ray halos around pulsars, suppresses the overall amplitude of the background component.

Our model is quite simple, and well-motivated by up-to-date precise observations of GCRs and γ -rays. In particular, the common energy scale appeared in both the monopole (spectra) and dipole (anisotropies) can be naturally explained in this model. We link the anisotropy spectral evolution with the particle spectra, which show the same characteristic energy scale. Importantly, our scenario provides a new way to pinpoint the sources of GCRs via spectral features of both the fluxes and the anisotropies, which could be applied further to the energy range above the knee.

Acknowledgments

This work is supported by the National Key Research and Development Program of China (No. 2016YFA0400200), the National Natural Science Foundation of China (Nos. 11875264, 11635011, 11663006, 11761141001, 11722328, 11851305), and the 100 Talents program of Chinese Academy of Sciences.

References

- [1] A. R. Bell. The acceleration of cosmic rays in shock fronts. I. *MNRAS*, 182:147–156, January 1978.
- [2] R. D. Blandford and J. P. Ostriker. Particle acceleration by astrophysical shocks. *ApJ*, 221:L29–L32, April 1978.
- [3] M. Aguilar, L. Ali Cavazonza, G. Ambrosi, et al. Observation of New Properties of Secondary Cosmic Rays Lithium, Beryllium, and Boron by the Alpha Magnetic Spectrometer on the International Space Station. *Physical Review Letters*, 120(2):021101, January 2018.
- [4] Q. Yuan, S.-J. Lin, K. Fang, and X.-J. Bi. Propagation of cosmic rays in the AMS-02 era. *Phys. Rev. D*, 95(8):083007, April 2017.

- [5] A. W. Strong, I. V. Moskalenko, and V. S. Ptuskin. Cosmic-Ray Propagation and Interactions in the Galaxy. *Annual Review of Nuclear and Particle Science*, 57:285–327, November 2007.
- [6] M. Aglietta, B. Alessandro, P. Antonioli, et al. A Measurement of the Solar and Sidereal Cosmic-Ray Anisotropy at E 0 approximately 10 14 eV. *ApJ*, 470:501, October 1996.
- [7] M. Amenomori, S. Ayabe, X. J. Bi, et al. Anisotropy and Corotation of Galactic Cosmic Rays. *Science*, 314:439–443, October 2006.
- [8] M. Aglietta, V. V. Alekseenko, B. Alessandro, et al. Evolution of the Cosmic-Ray Anisotropy Above 10^{14} eV. *ApJ*, 692:L130–L133, February 2009.
- [9] M. G. Aartsen, K. Abraham, M. Ackermann, et al. Anisotropy in Cosmic-Ray Arrival Directions in the Southern Hemisphere Based on Six Years of Data from the IceCube Detector. *ApJ*, 826:220, August 2016.
- [10] M. Amenomori, X. J. Bi, D. Chen, et al. Northern Sky Galactic Cosmic Ray Anisotropy between 10 and 1000 TeV with the Tibet Air Shower Array. *ApJ*, 836:153, February 2017.
- [11] C. Evoli, D. Gaggero, D. Grasso, and L. Maccione. Common Solution to the Cosmic Ray Anisotropy and Gradient Problems. *Physical Review Letters*, 108(21):211102, May 2012.
- [12] A. D. Panov, J. H. Adams, H. S. Ahn, et al. Energy spectra of abundant nuclei of primary cosmic rays from the data of ATIC-2 experiment: Final results. *Bulletin of the Russian Academy of Sciences, Physics*, 73:564–567, June 2009.
- [13] H. S. Ahn, P. Allison, M. G. Bagliesi, et al. Discrepant Hardening Observed in Cosmic-ray Elemental Spectra. *ApJ*, 714:L89–L93, May 2010.
- [14] O. Adriani, G. C. Barbarino, G. A. Bazilevskaya, et al. PAMELA Measurements of Cosmic-Ray Proton and Helium Spectra. *Science*, 332:69–, April 2011.
- [15] M. Aguilar, D. Aisa, B. Alpat, et al. Precision Measurement of the Proton Flux in Primary Cosmic Rays from Rigidity 1 GV to 1.8 TV with the Alpha Magnetic Spectrometer on the International Space Station. *Physical Review Letters*, 114(17):171103, May 2015.

- [16] R. Yang, F. Aharonian, and C. Evoli. Radial distribution of the diffuse γ -ray emissivity in the Galactic disk. *Phys. Rev. D*, 93(12):123007, June 2016.
- [17] F. Acero, M. Ackermann, M. Ajello, et al. Development of the Model of Galactic Interstellar Emission for Standard Point-source Analysis of Fermi Large Area Telescope Data. *ApJS*, 223:26, April 2016.
- [18] N. Tomassetti. Origin of the Cosmic-Ray Spectral Hardening. *ApJ*, 752:L13, June 2012.
- [19] Y.-Q. Guo and Q. Yuan. Understanding the spectral hardenings and radial distribution of Galactic cosmic rays and Fermi diffuse γ rays with spatially-dependent propagation. *Phys. Rev. D*, 97(6):063008, March 2018.
- [20] Y. S. Yoon, T. Anderson, A. Barrau, et al. Proton and Helium Spectra from the CREAM-III Flight. *ApJ*, 839:5, April 2017.
- [21] E. Atkin, V. Bulatov, V. Dorokhov, et al. New Universal Cosmic-Ray Knee near a Magnetic Rigidity of 10 TV with the NUCLEON Space Observatory. *Soviet Journal of Experimental and Theoretical Physics Letters*, 108:5–12, July 2018.
- [22] M. Amenomori and Tibet $\text{As}\gamma$ Collaboration. Modeling of the high-energy galactic cosmic-ray anisotropy. *Astrophysics and Space Sciences Transactions*, 6:49–52, December 2010.
- [23] N. A. Schwadron, F. C. Adams, E. R. Christian, et al. Global Anisotropies in TeV Cosmic Rays Related to the Sun’s Local Galactic Environment from IBEX. *Science*, 343:988–990, February 2014.
- [24] V. Savchenko, M. Kachelrieß, and D. V. Semikoz. Imprint of a 2 Million Year Old Source on the Cosmic-Ray Anisotropy. *ApJ*, 809:L23, August 2015.
- [25] M. Ahlers. Deciphering the Dipole Anisotropy of Galactic Cosmic Rays. *Physical Review Letters*, 117(15):151103, October 2016.
- [26] P. Mertsch and S. Funk. Solution to the Cosmic Ray Anisotropy Problem. *Physical Review Letters*, 114(2):021101, January 2015.
- [27] A. D. Erlykin and A. W. Wolfendale. The anisotropy of galactic cosmic rays as a product of stochastic supernova explosions. *Astroparticle Physics*, 25:183–194, April 2006.

- [28] P. Blasi and E. Amato. Diffusive propagation of cosmic rays from supernova remnants in the Galaxy. I: spectrum and chemical composition. *J. Cosmology Astropart. Phys.*, 1:010, January 2012.
- [29] P. Blasi and E. Amato. Diffusive propagation of cosmic rays from supernova remnants in the Galaxy. II: anisotropy. *J. Cosmology Astropart. Phys.*, 1:11, January 2012.
- [30] M. Pohl and D. Eichler. Understanding TeV-band Cosmic-Ray Anisotropy. *ApJ*, 766:4, March 2013.
- [31] L. G. Sveshnikova, O. N. Strelnikova, and V. S. Ptuskin. Spectrum and anisotropy of cosmic rays at TeV-PeV-energies and contribution of nearby sources. *Astroparticle Physics*, 50:33–46, December 2013.
- [32] R. Kumar and D. Eichler. Large-scale Anisotropy of TeV-band Cosmic Rays. *ApJ*, 785:129, April 2014.
- [33] A. U. Abeysekara, A. Albert, R. Alfaro, et al. Extended gamma-ray sources around pulsars constrain the origin of the positron flux at Earth. *Science*, 358:911–914, November 2017.
- [34] Q. Yuan. Implications on cosmic ray injection and propagation parameters from Voyager/ACE/AMS-02 nucleus data. *Science China Physics, Mechanics, and Astronomy*, 62:49511, April 2019.
- [35] I. A. Grenier, J. H. Black, and A. W. Strong. The Nine Lives of Cosmic Rays in Galaxies. *ARA&A*, 53:199–246, August 2015.
- [36] Wei Liu, Yu-hua Yao, and Yi-Qing Guo. Revisiting Spatial-Dependent Propagation Model with Latest Observations of Cosmic Ray Nuclei. *arXiv e-prints*, page arXiv:1802.03602, February 2018.
- [37] G. Case and D. Bhattacharya. Revisiting the galactic supernova remnant distribution. *A&AS*, 120:437–440, December 1996.
- [38] C. Evoli, D. Gaggero, D. Grasso, and L. Maccione. Cosmic ray nuclei, antiprotons and gamma rays in the galaxy: a new diffusion model. *J. Cosmology Astropart. Phys.*, 10:018, October 2008.
- [39] W. D. Apel, J. C. Arteaga-Velázquez, K. Bekk, et al. KASCADE-Grande measurements of energy spectra for elemental groups of cosmic rays. *Astroparticle Physics*, 47:54–66, July 2013.

- [40] Yi-Qing Guo and Qiang Yuan. On the knee of galactic cosmic rays in light of sub-tev spectral hardenings. *Chinese Physics C*, 42(7):075103, 2018.
- [41] Bing-Qiang Qiao, Wei Liu, Yi-Qing Guo, and Qiang Yuan. Anisotropies of different mass compositions of cosmic rays. *arXiv e-prints*, page arXiv:1905.12505, May 2019.
- [42] V. V. Smith, K. Cunha, and B. Plez. Is Geminga a runaway member of the Orion association? *A&A*, 281:L41–L44, January 1994.
- [43] R. N. Manchester, G. B. Hobbs, A. Teoh, and M. Hobbs. The Australia Telescope National Facility Pulsar Catalogue. *AJ*, 129:1993–2006, April 2005.
- [44] J. Faherty, F. M. Walter, and J. Anderson. The trigonometric parallax of the neutron star Geminga. *Ap&SS*, 308:225–230, April 2007.
- [45] M. Aguilar, L. Ali Cavazonza, B. Alpat, et al. Observation of the Identical Rigidity Dependence of He, C, and O Cosmic Rays at High Rigidities by the Alpha Magnetic Spectrometer on the International Space Station. *Physical Review Letters*, 119(25):251101, December 2017.
- [46] E. Atkin, V. Bulatov, V. Dorokhov, et al. First results of the cosmic ray NUCLEON experiment. *J. Cosmology Astropart. Phys.*, 7:020, July 2017.
- [47] T. Antoni, W. D. Apel, A. F. Badea, et al. KASCADE measurements of energy spectra for elemental groups of cosmic rays: Results and open problems. *Astroparticle Physics*, 24:1–25, September 2005.
- [48] M. Ahlers and P. Mertsch. Origin of small-scale anisotropies in Galactic cosmic rays. *Progress in Particle and Nuclear Physics*, 94:184–216, May 2017.
- [49] J. R. Hörandel. On the knee in the energy spectrum of cosmic rays. *Astroparticle Physics*, 19:193–220, May 2003.
- [50] D. Hooper, I. Cholis, T. Linden, and K. Fang. HAWC observations strongly favor pulsar interpretations of the cosmic-ray positron excess. *Phys. Rev. D*, 96(10):103013, November 2017.
- [51] K. Fang, X.-J. Bi, P.-F. Yin, and Q. Yuan. Two-zone Diffusion of Electrons and Positrons from Geminga Explains the Positron Anomaly. *ApJ*, 863:30, August 2018.

- [52] O. Adriani, G. C. Barbarino, G. A. Bazilevskaya, et al. An anomalous positron abundance in cosmic rays with energies 1.5-100GeV. *Nature*, 458:607–609, April 2009.
- [53] M. Aguilar, G. Alberti, B. Alpat, et al. First Result from the Alpha Magnetic Spectrometer on the International Space Station: Precision Measurement of the Positron Fraction in Primary Cosmic Rays of 0.5-350 GeV. *Physical Review Letters*, 110(14):141102, April 2013.
- [54] Q. Yuan and L. Feng. Dark Matter Particle Explorer observations of high-energy cosmic ray electrons plus positrons and their physical implications. *Science China Physics, Mechanics, and Astronomy*, 61:101002, October 2018.